# Simplifying Kinematic Parameter Estimation in sEMG Prosthetic Hands: A Two-Point Approach

Gang Liu, Zhenxiang Wang, Ziyang He, Shanshan Guo, Rui Zhang, Dezhong Yao

Abstract—Regression-based sEMG prosthetic hands are widely used for their ability to provide continuous kinematic parameters. However, establishing these models traditionally requires complex kinematic sensor systems to collect corresponding kinematic data in synchronization with EMG, which is cumbersome and userunfriendly. This paper presents a simplified approach utilizing only two data points to depict kinematic parameters. Finger flexion is recorded as 1, extension as -1, and a near-linear model is employed to interpolate intermediate values, offering a viable alternative for kinematic data. We validated the approach with twenty participants through offline analysis and online experiments. The offline analysis confirmed the model's capability to fill in intermediate points, and the online experiments demonstrated that participants could control gestures, adjust force accurately. This study significantly reduces the complexity of collecting dynamic parameters in EMG-based regression prosthetics, thus enhancing usability for prosthetic hands.

*Index Terms*— myoelectric interface, prosthetic hand, electromyogram, real-time systems.

# I. INTRODUCTION

He motor unit (MU) is the smallest functional unit in the human neuromuscular system, which is composed of motor neurons and innervated muscle fibers[1]. By

This work is supported by the National Natural Science Foundation of China (62303423. 62373295), Postdoctoral Science Foundation of China (2023M733245), the Henan Province key research and development and promotion of special projects (242102311239), the ST! 2030-Major Project(2022ZD0208500), the Shanghai Key Laboratory of brain-computer Collaborative Information Behavior (2023KFKT005).

G Liu and R Zhang are School of Electrical and information Engineering, Zhengzhou University, Zhengzhou, 450001, China, and also with Henan Key Laboratory of Brain Science and Brain Computer Interface Technology, Zhengzhou University,450001, China.(e-mail:gangliu\_@zzu.edu.cn; ruizhang@zzu.edu.cn)

Z Wang is with Engineering Department of International College, Zhengzhou University,450001, China, and also with Henan Key Laboratory of Brain Science and Brain Computer Interface Technology, Zhengzhou University,450001, China. Z He is with School of Cyber Science and Engineering, Zhengzhou University, Zhengzhou, Henan 450000, China. S Guo is with Shanghai Key Laboratory of Brain-Machine Intelligence for Information Behavior, Shanghai International Studies University, Shanghai, 200083, China. (email:wzx3331@outlook.com;zyhe@zzu.edu.cn;guoshanshan@shisu.edu.cn)

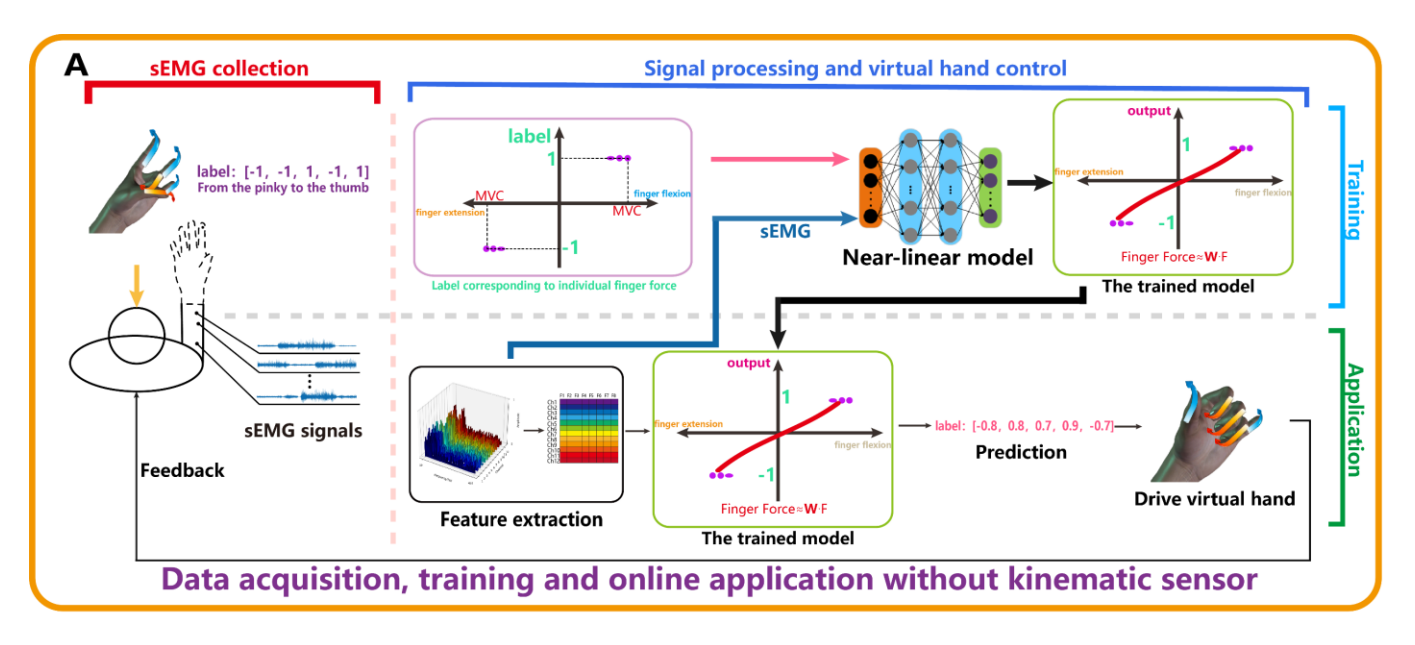
D Yao is with the Clinical Hospital of Chengdu Brain Science Institute, MOE Key Laboratory for NeuroInformation, School of Life Science and Technology, University of Electronic Science and Technology of China, Chengdu, 611731, China, and also with the Research Unit of NeuroInformation, Chinese Academy of Medical Sciences, Chengdu, 611731, China. (e-mail: dyao@uestc.edu.cn)

utilizing sensors to capture the action potentials of multiple MUs and processing them, we obtain the electromyographic (EMG) signal[2]. Therefore, EMG contains abundant movement information and has been widely applied to myoelectric control, particularly in prosthetics.[3-5].

1

With the rapid development of neural networks in recent years, the deep learning method of classification has been able to realize the recognition of various gestures effectively. Ulysse Côté-Allard *et al.* have aggregated sEMG data from multiple individuals to propose a classification method based on transfer learning[6]. Zhai, X.L *et al.* have introduced a self-recalibrating classifier using CNN[7], while Hu, Y *et al.* have developed an attention-based hybrid CNN-RNN architecture that better captures the temporal characteristics of sEMG signals[8]. However, the scope of application of classification methods is relatively limited, these methods only pay attention to the result of the movement, namely the formed gesture, but ignore the basic composition of the movement such as muscle connectivity to individual fingers, force, and speed.

In order to overcome the limitations of classification methods, many studies have applied regression methods or built more general models to decode the basic process of motion from EMG. Most of these studies have focused on predicting joint angles or estimating force and torque. In the estimation of finger force, Hang Su et al. constructed an algorithm to explore the potential model between sEMG and interaction force for human-robot interaction[9]. Gang Liu et al. presented a dynamic energy model that decodes continuous hand actions by training small amounts of sEMG data[10]. Yang Zheng and Xiaogang Hu proposed a neural-driven method for extracting MU discharge events from sEMG to achieve real-time estimation of finger force[11]. However, neither the finger force estimation method mentioned above, nor other joint angle prediction, has got rid of the use of kinematic sensors.[12-16], and some studies have adopted 3D motion camera system[17]. This reliance significantly increases system complexity and imposes high requirements for synchronization between kinematic data and sEMG data collection.



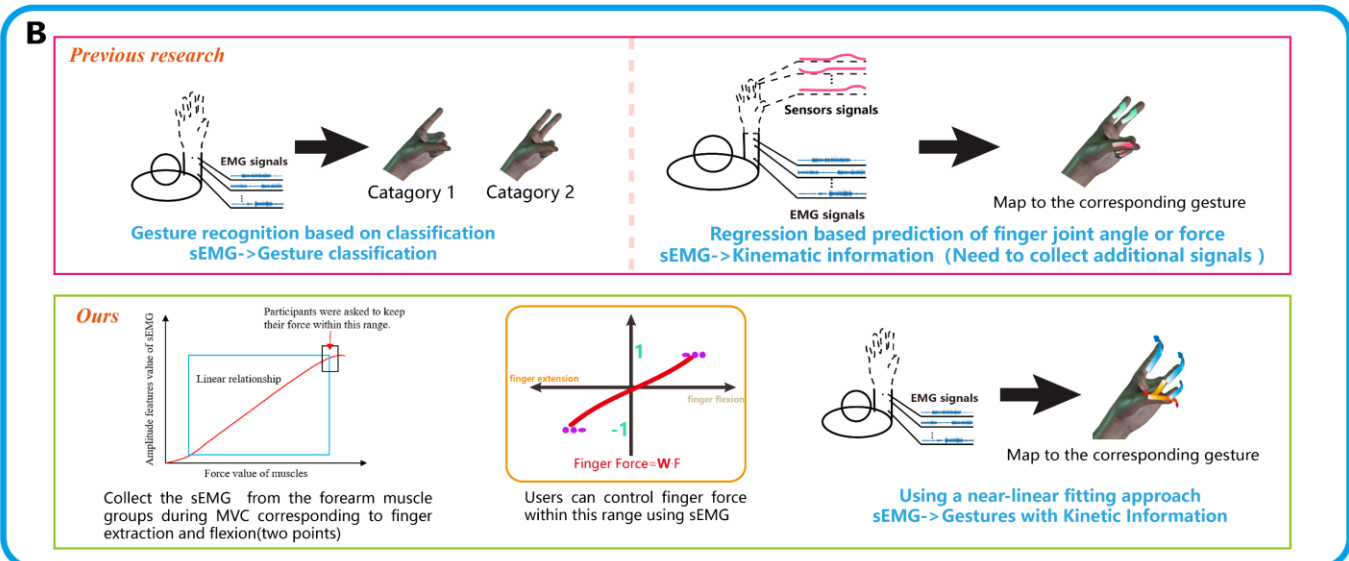


**Fig. 1.** Continuous prediction of finger force and virtual hand control system based on sEMG. Part A demonstrates the process of data acquisition, model training, and online application without the need for kinematic sensors; Part B contrasts the differences in methods for gesture recognition and kinematic information prediction between this study and previous research.

In this paper, we propose a two-point approach that capitalizes on the near-linear correlation between electromyography (EMG) and muscle force within a specific range and only needs to collect EMG data of two key points without additional sensors. We recorded the finger flexion as 1 and the finger extension as -1, and then used a near-linear model to fit and complete their intermediate values instead of the traditional kinematic parameters. In this way, the magnitude of force and speed of the finger can be decoded in real-time, and then used for prosthetic hand control.

The rest of the paper is organized as follows: Section II

describes the establishment of the model in detail, including data collection, signal preprocessing, data set establishment methods and the structure of the model. Section III describes the experimental methods and the statistical analysis of the results. Furthermore, our work is discussed in Section IV. Finally, Section V concludes this work and outlines future research directions.

# II. METHODOLOGY

- A. Inspiration and Model Derivation
- 1) Inspiration

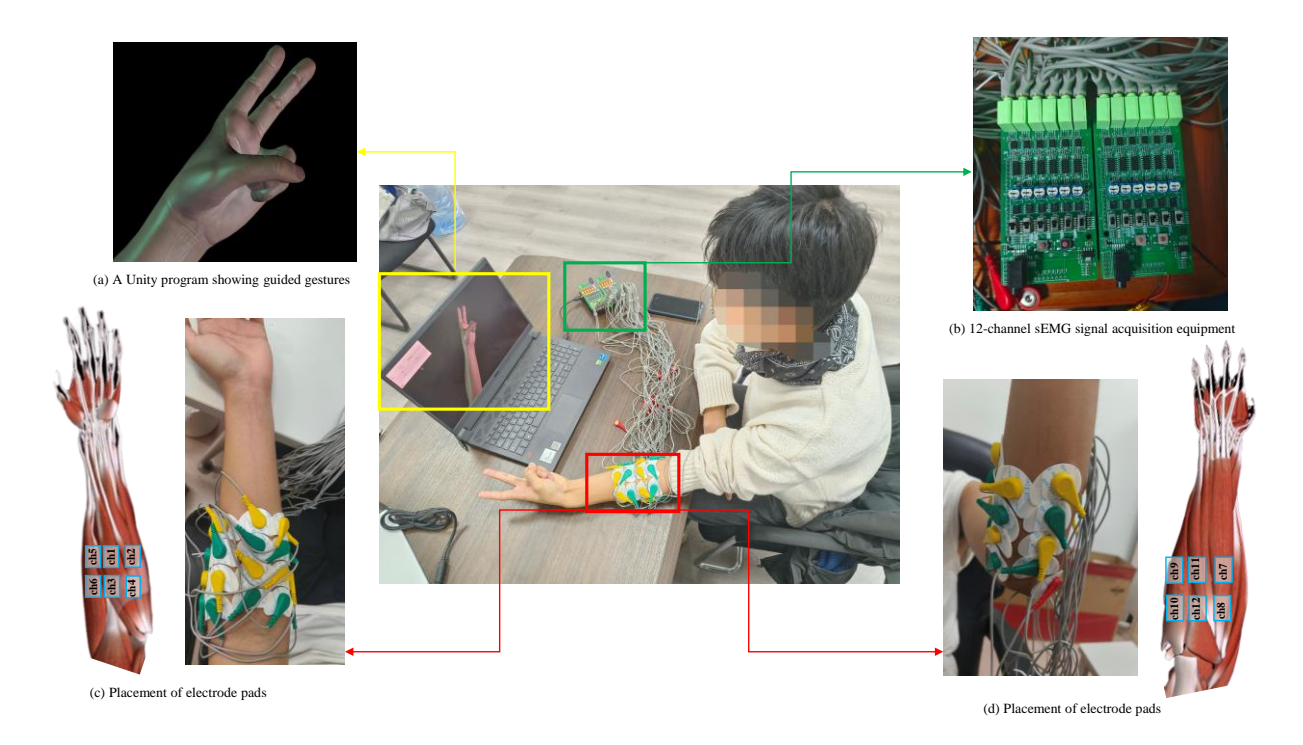


**Fig. 2.** sEMG data collection as shown in the figure, we used a 12-channel sensor to collection raw sEMG data, and covered the muscle groups of the forearm as much as possible, and used the Unity 3D program to display guided gestures.

Previous studies have shown that, within a certain range, the force value of a muscle has a near-linear correlation with the characteristic value of its corresponding sEMG signal[18-22]. This allows us to model other force values within the linear region by simply scaling the extreme values of the force output within the linear relationship. During maximal finger extension and flexion, the forearm muscle groups responsible for these movements perform isometric contractions that produce maximal force while maintaining a constant muscle length. These maximal voluntary contractions(MVC) produce discernible surface electromyographic signals[23]. Although the relationship between muscle force and sEMG signal is not entirely linear at MVC of the muscle, the sEMG signal recorded during MVC can be used as an approximate indicator of the muscle's force output at the upper limit of the linear To capture sEMG signals representing maximal interval. muscle force, participants were instructed to maintain maximal gestures, thereby recording sEMG signals near the endpoints of the linear force-sEMG relationship.

# 2) Model Derivation

In our study, we establish two anchor points based on the MVCs during finger extension and finger flexion. Each MVC is associated with specific forearm muscle groups responsible for the different movements. These two extreme conditions of muscle contraction allow us to capture the sEMG signals that closely represent the high end of the muscle force spectrum.

We employed a 12-channel electromyography device to record sEMG signals from the forearm muscles responsible for finger movements. Each muscle group was associated with one or multiple channels. Denoting the sEMG signals from per channel as  $s_i$ , we obtain windowed data  $w_{i,n}$ , with n

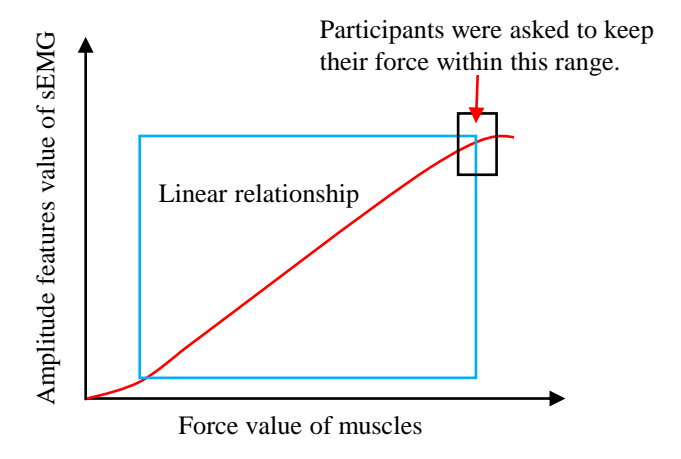


**Fig. 3.** Relationship between force value of muscles and amplitude features value of sEMG.

indexing the window number within the channel i. For each windowed segment  $W_{i,n}$ , a set of m features is extracted, resulting in a feature vector  $f_{i,n}$ . The feature extraction process transforms each windowed segment into an m-dimensional feature space, hereby constructing a feature matrix  $F_i$  for each channel:

$$F_{i} = \left[ f_{i,2}^{T}, f_{i,2}^{T}, \dots, f_{i,N}^{T} \right]^{T}$$
 (1)

where N is the total number of windows extracted from each channel. The feature matrices from all 12 channels are concatenated to form a comprehensive feature tensor  $\boldsymbol{F}$  of size  $N \times 12 \times m$ .

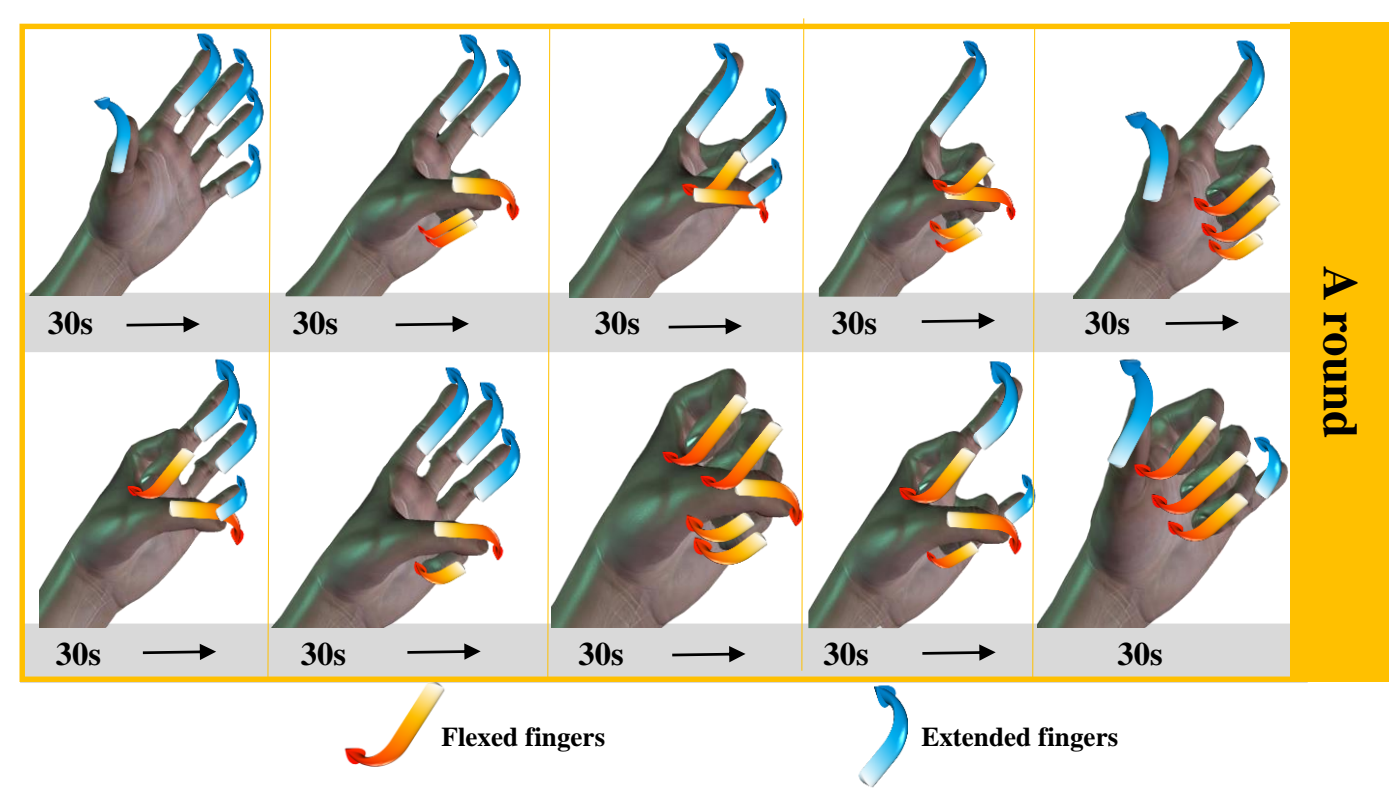


Fig. 4. List of the 10 gestures in source gesture set and their force mode, participants hold each gesture for 30 seconds.

The relationship between surface EMG and finger force of forearm muscles is assumed to be an approximate linear model and can be expressed as:

Force 
$$\approx \mathbf{W} \cdot \text{vec}(\mathbf{F})$$
 (2)

where  $\mathbf{W}$  is a matrix of coefficients,  $\operatorname{vec}(F)$  is the vectorization of the feature tensor F. Our aim is to employ regression techniques from machine learning to determine the parameters  $\mathbf{W}$ . This two-point approach allows us to interpolate force values for sEMG activities lying between the two MVC conditions, thus can predict the finger force output, including the direction and approximate speed of finger movement, simplifying computational complexity and eliminating the dependence on kinematic sensors.

# B. sEMG Data Acquisition

Different gestures are implemented by different finger force patterns. In order to ensure that these gestures include the extension and flexion movements of five fingers, we designed ten gestures as source gesture sets as shown in **Fig. 4.** 

In this study, twenty able-bodied subjects (two females, eighteen males, aged  $19.5 \pm 1.05$  years) gave informed consent to participate in the experiment protocol. All participants were right-handed and without any history of neurological or muscular diseases. The EMG signals were recorded from the left forearm of the participants. The study protocol was approved by the ethics review board. All procedures performed in the study were in accordance with the Declaration of Helsinki and relevant policies.

We utilized a 12-channel sEMG acquisition system paired with a PC, with a sampling rate set to 1 kHz. The real-time reading of sEMG data transmitted via the serial port was facilitated using Python, which allowed for the immediate processing of the incoming signals. Ag/AgCl gel electrodes with a 25 mm spacing were employed to capture the sEMG signals, with the electrode patches positioned to cover the entire muscle group of the forearm as comprehensively as possible.

Participants were seated in a comfortable chair with their left arm placed on a table. They were instructed to perform ten predefined gestures, which were displayed on a monitor screen. Each gesture was held for 30 seconds and counted as one set. Every participant repeated the set of gestures three times, with a five-minute rest interval between each set to minimize muscle fatigue[19]. This procedure ensured that a complete set of sEMG signals was collected for each gesture. The collected sEMG data from all subjects were then prepared for offline analysis to investigate the different finger force.

## C. Signal Preprocessing and Feature Extraction

After recording the sEMG signals, we combined the three sets of data from each participant to increase the overall dataset, resulting in one comprehensive dataset per person for training purposes. In most ranges of muscle force generation, it has a linear relationship with the amplitude features of the corresponding sEMG. Therefore, to simulate different muscle force levels, the original sEMG data was scaled down to between 0.1 and 0.9 of the original amplitude in increments of 0.1. This scaled data was used as the test set (see **Fig.6**).

TABLE I
FEATURES AND FORMULAS

FEATURES AND FORMULAS				
Feature name and their abbreviation	Formula			
Root Mean Square (RMS)	$\sqrt{\frac{1}{N}\sum_{i=1}^{N}x_{i}^{2}}$			
Mean Absolute Value (MAV)	$\frac{1}{N}\sum_{i=1}^{N} x_{i} $			
Variance (VAR)	$\frac{1}{N-1} \sum_{i=1}^{N} (x_i - \overline{x})^2$			
Standard Deviation (SD)	$\sqrt{\frac{1}{N-1}\sum_{i=1}^{N}(x_i-\overline{x})^2}$			
Integral (INT)	$\sum_{i=1}^{N}  x_i $			
Wavelength (WL)	$\sum_{i=1}^{N-1}  x_{i+1} - x_i $			
Difference Absolute Standard Deviation Value	$\sqrt{\frac{1}{N-1}\sum_{i=1}^{N-1}(x_{i+1}-x_i)^2}$			
(DASDV)	$\sqrt{N-1}\sum_{i=1}^{N-1}$			
Difference Absolute Mean	$\frac{1}{N-1} \sum_{i=1}^{N-1}  x_{i+1} - x_i $			
Value (DAMV)	$N-1$ $\sum_{i=1}^{N-1} N_i + i$			

Since the sEMG signal is extremely weak, it is easy to be disturbed by noise from various sources such as skin, sensors, and the environment. In order to improve the analyzability of the electromyography signal, we must first preprocess it[24]. Firstly, we removed the direct current (DC) component from the 12-channel sEMG data to eliminate any baseline drift[25]. Then, we individually filtered each channel with a 6th order Butterworth bandpass filter from 10 Hz to 450 Hz to remove motion artifacts and high-frequency noise, ensuring that differences in electrode placement do not affect the sEMG signals[25]. A 50 Hz notch filter was also applied to each channel to eliminate power line interference [26]. After filtering, we performed full-wave rectification on the data. For real-time force analysis, low latency and fast response are necessary, and smaller Windows can achieve this. Therefore, we processed all data using a sliding window approach with a 200ms window length and a 50ms step size[27].

In order to obtain useful information in sEMG and eliminate interfering components, it is necessary to carry out feature extraction. Conventional sEMG signal features include

TABLE II MODELS AND THEIR ORDER

Туре	Models	Core Formulas	Systems Fit by the Model
Near- linear model	DD	$G = WX$ $Y = G \circ X + G$	Second- order system (one- layer DD)
	LN	Y = WX	first- order system
Nonlinear complex model	MLP	Y = ReLU(WX + b)	High- order system
	CNN	$C = \text{ReLU} \left[ \text{Conv}_{2D} \left( X \right) \right]$ $P = \text{Pool} \left( C \right)$ $Y = \text{ReLU} \left( WP + b \right)$	High- order system

time domain features, frequency domain features, timefrequency domain features [28, 29]. In our two-point approach, the most critical is the use of linear relationship segments, so we extracted eight time-domain amplitude features shown in TABLE I from each channel of the sEMG data: Root Mean Square (RMS), Mean Absolute Value (MAV), Variance (VAR), Standard Deviation (SD), Integral (INT), Wavelength (WL), Difference Absolute Standard Deviation Value (DASDV), and Difference Absolute Mean Value (DAMV). According to the formulas listed in TABLEI, we can infer that the values of these features have a monotonically increasing relationship with the values of the original signal sequence  $X_i$ . Therefore, after scaling the original EMG signals, the scaling relationship will still be preserved in the feature values. And the per-channel feature extraction processing can avoid the differences introduced by variations in electrode patch placement, providing a detailed and robust dataset for analyzing muscle force.

## D. Specific Model

Based on the Model Derivation section above, we need a model capable of near-linear fitting to meet our linear control requirements. Therefore, we use Dendritic Net (DD) to implement the two-point approach, and use a fully linear network (LN), multi-layer perceptron (MLP) and

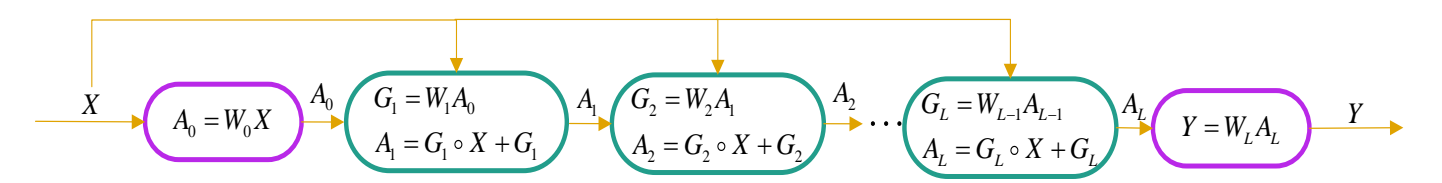


**Fig. 5.** DD structure with the residual connections.

Fig. 6. Offline analysis flow diagram

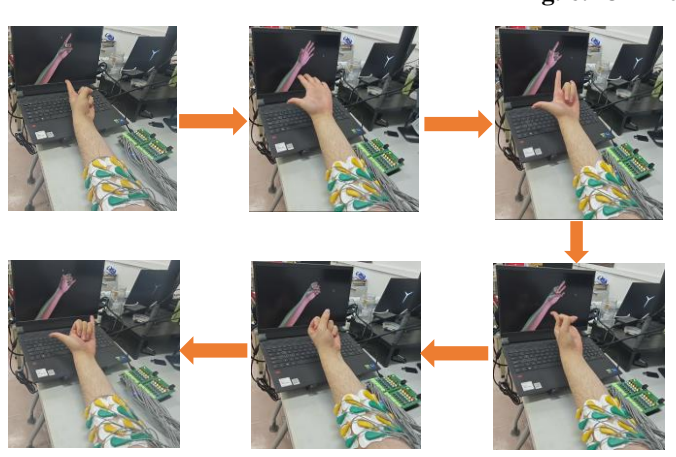


Fig. 7. Real-time control of virtual

convolutional neural network (CNN) for performance comparison.

# 1) Near-linear model

><

DD is a new type of white-box neural network inspired by the dendritic structure of the brain. Our model uses an improved DD, which introduces some special residual connections and contains one layers of DD modules[30, 31]. Its network structure is shown in **Fig. 5.** By adjusting the number of DD modules, the logical expression ability of the algorithm and the order of its fitting system can be effectively adjusted[32-34]. Its model is capable of fitting up to a second-order system. Its formula can be seen in the TABLEII, and the one-layer DD model is capable of fitting up to a second-order system. Its excellent generalization ability and low computational complexity are the main reasons for our choice. While the LN represents a network composed entirely of fully connected layers, and the fully connected layers do not have biases.

# 2) Nonlinear model

In our study, we selected two nonlinear model representatives, MLP and CNN, whose core formulas are shown in the TABLEII. The MLP incorporates activation

functions such as Sigmoid, ReLU, tanh, etc. (ReLU is used in this study) into the fully connected layers, enabling it to capture complex relationships between inputs and outputs. The CNN uses convolutional kernels for a certain degree of feature extraction from the inputs, known as convolutional layers, followed by activation functions and pooling for dimensionality reduction [35-37]. Finally, fully connected layers are used for the output. Both MLP and CNN can implement many relatively complex mappings, but they find it difficult to achieve linear fitting.

# 3) Specific models in the experiments

We use a random number seed (random state=42) to split the unscaled data set, randomly assign one-third as the test set, and the remaining two-thirds as the training set and validation set for ten-fold cross-validation, and shuffle the training data. The LN in the comparison experiment only uses three fully connected layers, including an input layer and an output layer and a hidden layer, and sets the Bias of these fully connected layers to false. The network structure of MLP is three fully connected layers, and ReLU activation is used after the input layer and hidden layer. While CNN uses 2 convolutional layers, 1 max pooling layer and the last 2 fully connected layers, the ReLU activation function is used after the convolutional layer and the first fully connected layer. All data are normalized before input, and neither DD nor LN uses activation functions, and none of the four machine learning algorithms uses activation functions at the output layer. The loss function is the mean square error (MSE), using the Adam optimizer with a learning rate of 0.002. Each fold is trained for 15 epochs, and average loss on the validation set is saved. We built unique models for each subject, which will be used for subsequent offline analysis and online experiments.

# III. EXPERIMENT RESULTS AND ANALYSIS

We design offline analysis and online experiments to verify the performance of our model. The flow of offline analysis test is shown in **Fig. 6.** Real-time control of virtual hand experiment is shown in **Fig. 7.** 

TABLE III OFFLINE ANALYSES RESULTS

Output Method		Area Under the Curve (AUC)	Standard Error (SE)	Asymptotic 95% Confidence Interval (CI)		Accuracy
	DD	0.977887	0.000449	0.977859	0.977859 0.977916	
L1	LN	0.929772	0.000804	0.929722	0.929823	85.01%
	MLP	0.993835	0.000250	0.993819	0.993850	96.63%
	CNN	0.999411	0.000073	0.999407	0.999416	99.15%
L2	DD	0.972789	0.000552	0.972754	0.972824	90.84%
	LN	0.942453	0.000798	0.942402	0.942503	86.07%
	MLP	0.988339	0.000382	0.988315	0.988363	94.50%
	CNN	0.998866	0.000113	0.998859	0.998873	98.66%
L3	DD	0.982602	0.000398	0.982577	0.982627	93.79%
	LN	0.968013	0.000541	0.967979	0.968047	91.45%
	MLP	0.992689	0.000272	0.992672	0.992706	96.18%
	CNN	0.999116	0.000089	0.999111	0.999122	98.85%
L4	DD	0.967460	0.000506	0.967429	0.967492	90.94%
	LN	0.919576	0.000812	0.919525	0.919627	84.78%
	MLP	0.989969	0.000292	0.989951	0.989987	95.55%
	CNN	0.999032	0.000086	0.999026	0.999037	98.84%
L5	DD	0.980862	0.000529	0.980829	0.980895	93.94%
	LN	0.955773	0.000797	0.955723	0.955822	90.28%
	MLP	0.992517	0.000351	0.992495	0.992539	96.65%
	CNN	0.998840	0.000131	0.998832	0.998848	98.97%

## A. Offline analysis

In our model, the output value represents the force exerted, and the positive and negative represent the direction, that is, whether the finger is flexion or extension.

We obtain the corresponding five sets of outputs (L1, L2, L3, L4, L5) of the test set for each subject, and merge them to obtain all the outputs of the corresponding five fingers across all subjects. The output value 0 of the model is the threshold for distinguishing the direction of finger force, so 0 is used as the threshold for accuracy calculation. To verify the model's ability to learn and decode sEMG information accurately, we conducted offline analyses using the Area Under the Curve (AUC) metric. We trained four different machine learning models (DD, LN, MLP and CNN) on the unscaled dataset and evaluated their performance in classifying finger force direction. After statistical testing, the Receiver Operating Characteristic (ROC) curve shown in Fig. 8. and analysis (p<0.001) shown in TABLE III demonstrate the good performance of the model in the prediction of finger force direction. The accuracy of the model is shown in TABLE III, we can see that our method achieves high accuracy across four machine learning methods, while more complex networks like CNN and MLP demonstrate better classification accuracy for finger force direction.

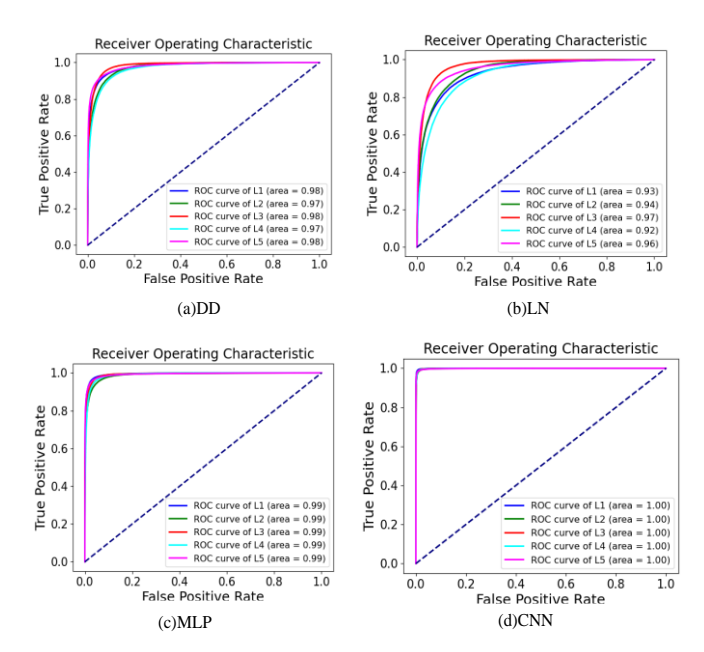


**Fig. 8.** The ROC curves corresponding to the four neural networks. From L1 to L5, represent pinky to thumb.

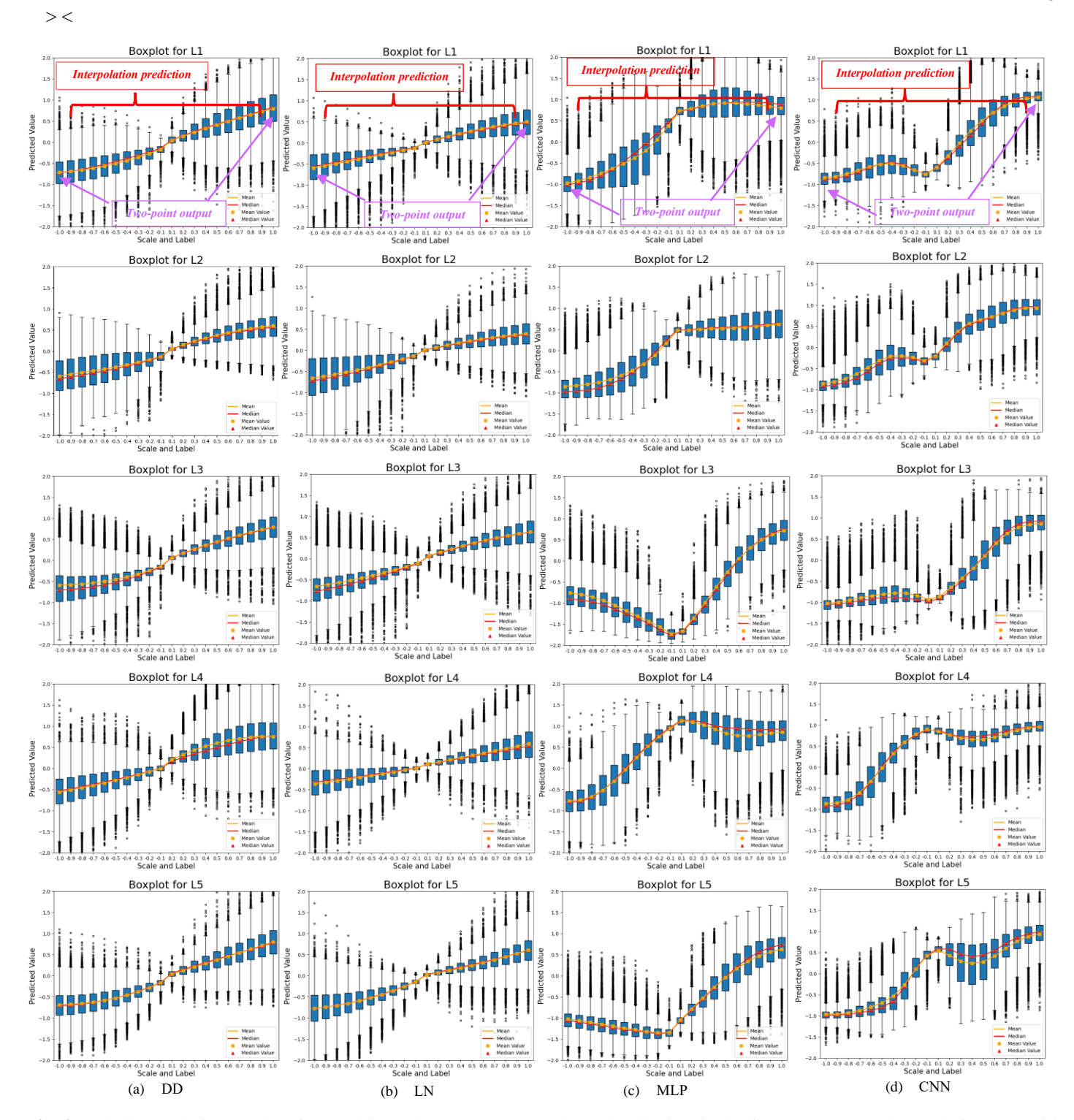


**Fig. 9.** The interpolation results of one subject's data are representative. The abscissa in the figure represents the scale factor. Positive values represent the finger extension, and negative values represent the finger bending. (c) and (d) show errors in which linear fitting cannot be achieved. The two ends of each image are the output of two points, corresponding to the analysis results of **Fig. 8** and TABLE III, and the output of model interpolation is in the middle. From L1 to L5, represent pinky to thumb.

We further investigate the ability of the model to interpolate intermediate force values between two extreme values. We used data sets that previously scaled to simulate different muscle strength levels as test sets to test the fit of the model, and then observed their ability to predict force-sEMG relationships over the whole range. The interpolation results of

the data for one of the subjects is shown in Fig.9, which is representative.

From the interpolation results of all subjects, it can be inferred that the models fitted with DD and LN are nearly linear, and they complete the supplement of the median value, while MLP and CNN have difficulty in doing so, and have

some typical errors, which make them unable to achieve the magnitude control of the force in linear control (For example, (c) and (d) in Fig. 7). Interpolating fit plots for all subjects can be seen in the supplementary material.

We counted all the results of 20 subjects and the results are shown in TABLE IV. Among the 100 fitting results of each machine learning algorithm, DD made 2 errors and LN made 4 errors. MLP and CNN made 61 errors and 35 errors respectively (See supplementary material).

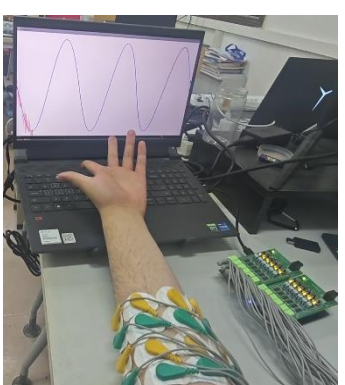
TABLE IV
STATISTICS ON THE NUMBER OF ERRORS IN FITTING RESULTS

Networks	DD	LN	MLP	CNN
Error Times	10	8	65	42
Correct rate	90%	92%	35%	58%

#### B. Online experiments

To evaluate the practicality of the model, we designed a sine-wave tracking experiment for online real-time control. Subjects wore a sEMG acquisition device and were asked to watch a static sine-wave on a screen, and then controlled the direction and size of the finger force at the same time to track the sine-wave on the screen as much as possible. At this time, sEMG would be input into the trained model after real-time processing. The program will draw a curve in real time based on the output of the model, and if the model works well, the curve drawn in real time should match the sine wave. The experiment was carried out in the form of single-finger control, that is, only the output of the corresponding finger was used to control each time. We selected the index finger and middle finger commonly used in life as the research object. Sine-wave tracking experiment is shown in **Fig. 10**.

The waveform diagram of the sine-wave tracking experiment of the index finger and middle finger is shown in f Fig. 11, and the statistical analysis is shown in Fig. 12. It can be seen that using MLP and CNN models, it is difficult to carry out real-time force control, and because the network structure is more complex than DD and LN, it also brings some challenges in time delay. The model using DD and LN could better complete the task and perform statistical analysis on the output during real-time control. The average Root-



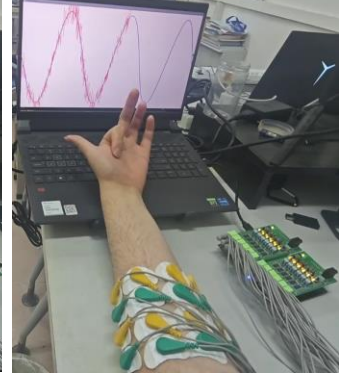


**Fig. 10.** Sine-wave tracking experiment

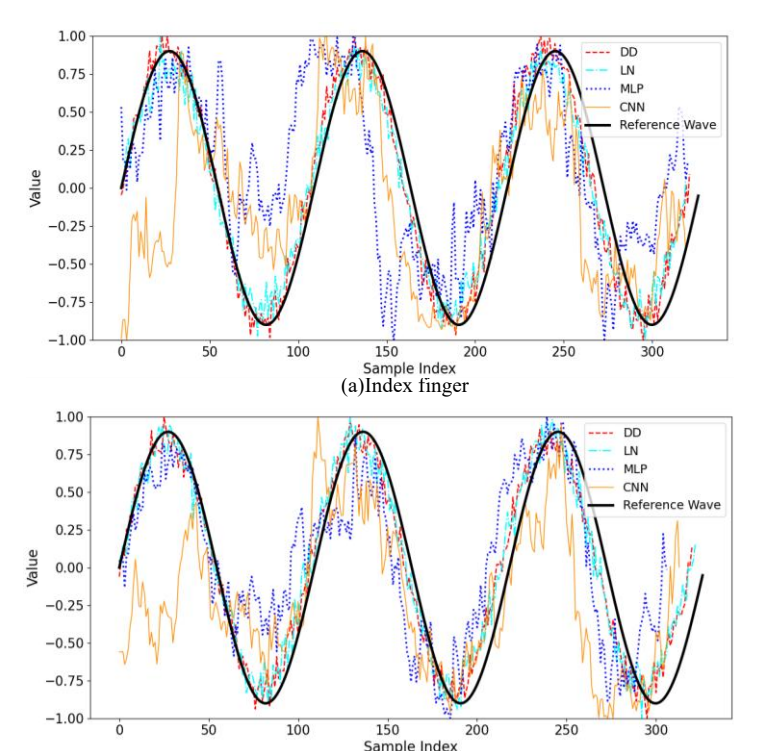


**Fig. 11.** Waveform diagram of the index and middle finger sinewave tracking experiment.

(b)Middle finger

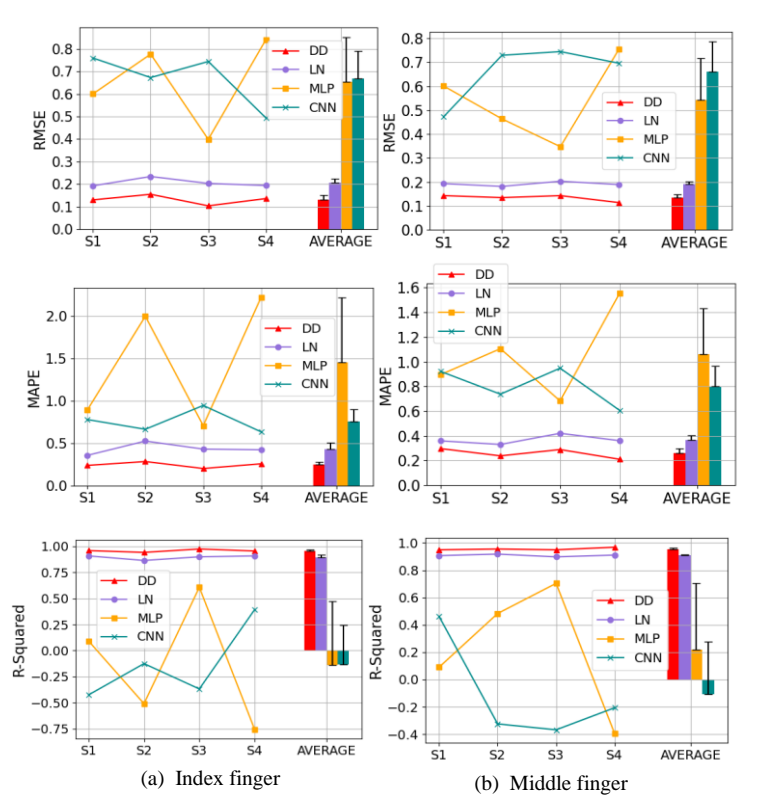


**Fig. 12.** Performance of RMSE, MAPE and R-squared in an online tracking reference sine-wave experiment with four subjects. The error bar represents the standard deviation (SD) between subjects.

Mean-Square Error (RMSE) on the index finger of the four subjects are 0.1311 and 0.2058, Mean Absolute Percentage Error (MAPE) are 0.2470 and 0.4359, and R-Squared are 0.9563 and 0.8937, respectively. On the middle finger, RMSE are 0.1331 and 0.1912, MAPE are 0.2580 and 0.3673, and R-Squared are 0.9553 and 0.9082, respectively.

In addition to the sine-wave tracking experiment, realtime control of all five fingers using our model was achieved in the Unity 3D program, and the five-finger control experiment can be seen in the supplementary video material.

## IV. DISCUSSION

In this study, we demonstrate that a model implemented using a two-point sEMG signal approach can be used to fit intermediate values to decode continuous hand movements with velocity or force information. By exploiting the nearlinear relationship between EMG amplitude and force output over a certain range, our approach eliminates the need for sensors applied to collect kinetic data. We conducted offline analysis and online experiments to verify the effectiveness of our method in accurately predicting force direction, fitting force-myoelectricity relationship, and controlling finger force in real time.

In the main direction of myoelectric interface research, most research is on the classification of gestures through pattern recognition[4-6]. These related works only focus on the gesture itself and ignore the movement itself. However, research on hand movements cannot avoid using of other kinematic parameters besides sEMG[12, 13]. Based on the work of predecessors, this paper starts from the sEMG signals of the muscle groups that control finger movement and uses only two points of data to simplify the process of decoding continuous finger force from the sEMG signals. This means that in future applications that use sEMG signals for hand movement control, the complexity of building systems can be simplified.

From the beginning of the design of the dataset, our gesture example included the extension and flexion states of all fingers, and subsequently discarded the sEMG signal when changing the gesture to avoid possible data leakage. The accuracy of the four machine learning methods in finger force direction classification is higher (DD: 92.35%, LN: 87.52%, MLP: 95.90%, CNN: 98.89%, five-finger average), indicating that the two-point method is effective in identifying finger force direction, and they capture the basic information needed for finger motion estimation from sEMG signals. In off-line analysis, the near-linear fitting results obtained by the DD and LN models demonstrate their ability to interpolate intermediate force values, which is crucial for accurately controlling the force magnitude and velocity of the prosthetic hand. In contrast, complex models such as MLP and CNN struggle to achieve this because they tend to overfit or exhibit uncontrollable behavior, making them unsuitable for interpolating intermediate value.

We can discuss this in terms of the structure of these networks. First, there are only fully connected layers in LN, and the output is a linear combination of inputs, given an input vector X with weight W , the output Y of LN can be expressed as:

$$Y = WX \tag{3}$$

This linear transformation preserves the monotonic relationship between input and output. If the input surface EMG signature has a near-linear relationship to the finger force, the LN will be able to capture and maintain this relationship, allowing for accurate interpolation of the intermediate force values. Compared with LN, the outputs of the first two layers of MLP are followed by ReLU activation functions. Given the input vector X, the one-layer output Y of an MLP with ReLU activation can be expressed as:

$$Y = \text{ReLU}(WX + b) \tag{4}$$

Where, W and b are the weight and bias of the layer respectively. The introduction of ReLU functions allows MLP to capture more complex relationships between inputs and outputs, which can fit training data more accurately, but is difficult to interpolate accurately[35, 36]. In our task, CNN is similar to MLP, although it introduces convolution computation and pooling operation to better capture useful information in the input, it has nonlinear activation function like MLP. We then discuss DD, which combines a linear transformation with a non-linear gating mechanism[30, 33, 37]. In the hidden layer of DD, given the output C of the input layer, the gating signal G:

$$G = W_{g}C \tag{5}$$

 $W_{\rm g}$  is the weight, and then the gating signal G is combined with the residual connection C to obtain the output Y of the DD layer.

$$Y = G \circ C + G \tag{6}$$

There are gating mechanisms and residual connections in DD, which combine linear transformation and nonlinear characteristics to preserve the linear relationship between input and output, while learning more complex relationships than LN. Regarding the fitting errors shown in the figures, theoretically DD and LN should not exhibit such errors. However, because the VAR value among the eight amplitude features we selected does not have a strictly linear relationship with the signal sequence values, for example, if the original sequence  $x_i$  has a VAR value of V, the VAR value after

scaling  $x_i$  by 0.7 would be 0.49V, which is a quadratic relationship. In addition, the reason why the number of errors in DD is slightly larger than that in LN may be that residual connection is introduced in DD we used, which introduces certain nonlinearity, but at the same time can capture more about the relationship between input and output, which is reflected in the better performance (shown in **Fig. 11** and **Fig. 12**) of DD in the sine-wave tracking experiment.

Online experiments further verify the practicality of our method in real-time control scenarios. Sine-wave tracking experiments demonstrate the ability of the DD and LN models to accurately control the direction and magnitude of finger force in real time. Both models achieve low RMSE and MAPE values, as well as high R-squared. Complex models such as

MLP and CNN face challenges in real-time force control due to the inability to interpolate intermediate values and the time delays introduced by more complex network structures. These results highlight the importance of model selection in real-time prosthetic control, where simplicity and interpretability are key factors.

The first limitation of our study is the lack of disabled subjects. However, previous studies have shown that amputees have similar muscle activation to non-disabled individuals[38, 39]. However, this study emphasizes the direct use of the sEMG signals of the forearm muscle groups that control the fingers when the fingers are at their maximum flexion and extension. Therefore, individuals with forearm muscles that can exert normal force can be candidates for this study.

Another difficulty is the coupling effect, when one finger moves, it will drive the other finger to move together, which will lead to changes in the sEMG of the corresponding muscle group[40, 41]. As for the thumb, the most special of the five fingers, because it has a large range of movement and can achieve many movements, it is a big challenge for electromyographic signal recognition.

#### V. CONCLUSION

In this paper, we propose a near-linear model based on sEMG and muscle forces to estimate continuous finger forces using two-point extremes, thus eliminating the need for dynamic sensors. The results show that: 1) The model designed by this method can learn the relationship between muscle activation and force, which is demonstrated by the high accuracy of finger force direction classification in offline analysis; 2) Analysis of simulated forces of different muscles shows that this monotonic relationship, combined with near-linear models (such as DD and LN), can effectively interpolate the intermediate force value, so as to achieve the control of the force size, while complex models with unlimited approximation ability, such as CNN and MLP, cannot insert the intermediate value due to the inability to control the order of the model; 3) Through the real-time control of the virtual hand experiment in Unity 3D and the single-finger sinusoidal tracking experiment, it has been demonstrated that our method has potential in prosthetic and finger control applications. The method shows that two extreme values can be used to fit the finger force between two points without the need for a dynamic sensor, thus simplifying the process of building a sEMG prosthetic hand.

# REFERENCES

- [1] D. S. de Oliveira *et al.*, "Neural decoding from surface high-density EMG signals: influence of anatomy and synchronization on the number of identified motor units," *Journal of Neural Engineering*, vol. 19, no. 4, Aug 2022, Art no. 046029, doi: 10.1088/1741-2552/ac823d.
- [2] D. Farina *et al.*, "The Extraction of Neural Information from the Surface EMG for the Control of Upper-Limb Prostheses: Emerging Avenues and Challenges," *IEEE Transactions on Neural Systems*

- and Rehabilitation Engineering, vol. 22, no. 4, pp. 797-809, 2014, doi: 10.1109/tnsre.2014.2305111.
- [3] H. Huang, F. Zhang, L. J. Hargrove, Z. Dou, D. R. Rogers, and K. B. Englehart, "Continuous Locomotion-Mode Identification for Prosthetic Legs Based on Neuromuscular-Mechanical Fusion," (in English), *IEEE Transactions on Biomedical Engineering*, Article vol. 58, no. 10, pp. 2867-2875, Oct 2011, doi: 10.1109/tbme.2011.2161671.
- [4] K. Kiguchi and Y. Hayashi, "An EMG-Based Control for an Upper-Limb Power-Assist Exoskeleton Robot," *Ieee Transactions on Systems Man and Cybernetics Part B-Cybernetics*, vol. 42, no. 4, pp. 1064-1071, Aug 2012, doi: 10.1109/tsmcb.2012.2185843.
- [5] M. Atzori, M. Cognolato, and H. Müller, "Deep Learning with Convolutional Neural Networks Applied to Electromyography Data: A Resource for the Classification of Movements for Prosthetic Hands," *Frontiers in Neurorobotics*, vol. 10, Sep 2016, Art no. 9, doi: 10.3389/fnbot.2016.00009.
- [6] U. Côté-Allard *et al.*, "Deep Learning for Electromyographic Hand Gesture Signal Classification Using Transfer Learning," *Ieee Transactions on Neural Systems and Rehabilitation Engineering*, vol. 27, no. 4, pp. 760-771, Apr 2019, doi: 10.1109/tnsre.2019.2896269.
- [7] X. L. Zhai, B. Jelfs, R. H. M. Chan, and C. Tin, "Self-Recalibrating Surface EMG Pattern Recognition for Neuroprosthesis Control Based on Convolutional Neural Network," *Frontiers in Neuroscience*, vol. 11, Jul 2017, Art no. 379, doi: 10.3389/fnins.2017.00379.
- [8] Y. Hu, Y. K. Wong, W. T. Wei, Y. Du, M. Kankanhalli, and W. D. Geng, "A novel attention-based hybrid CNN-RN N architecture for sEMG-based gesture recognition," *Plos One*, vol. 13, no. 10, Oct 2018, Art no. e0206049, doi: 10.1371/journal.pone.0206049.
- [9] H. Su, W. Qi, Z. Li, Z. Chen, G. Ferrigno, and E. De Momi, "Deep Neural Network Approach in EMG-Based Force Estimation for Human–Robot Interaction," *IEEE Transactions on Artificial Intelligence*, vol. 2, no. 5, pp. 404-412, 2021, doi: 10.1109/tai.2021.3066565.
- [10] G. Liu, L. Wang, and J. Wang, "A novel energy-motion model for continuous sEMG decoding: from muscle energy to motor pattern," *Journal of Neural Engineering*, vol. 18, no. 1, 2021, doi: 10.1088/1741-2552/abbece.
- [11] Y. Zheng and X. Hu, "Real-time isometric finger extension force estimation based on motor unit discharge information," *Journal of Neural Engineering*, vol. 16, no. 6, 2019, doi: 10.1088/1741-2552/ab2c55.
- [12] B. Lv, X. J. Sheng, W. C. Guo, X. Y. Zhu, and H. Ding, "Towards Finger Gestures and Force Recognition Based on Wrist Electromyography and Accelerometers," in 10th International Conference

- on Intelligent Robotics and Applications (ICIRA, Huazhong Univ Sci & Technol, Wuhan, PEOPLES R CHINA, Aug 16-18 2017, vol. 10462, in Lecture Notes in Artificial Intelligence, 2017, pp. 373-380, doi: 10.1007/978-3-319-65289-4\_36. [Online]. Available: <Go to ISI>://WOS:000725225700036
- [13] Y. Ban, "Estimating the Direction of Force Applied to the Grasped Object Using the Surface EMG," in 11th International Conference on Haptics Science, Technology, and Applications (EuroHaptics), Pisa, ITALY, Jun 13-16 2018, vol. 10894, in Lecture Notes in Computer Science, 2018, pp. 226-238, doi: 10.1007/978-3-319-93399-3\_21. [Online]. Available: <Go to ISI>://WOS:000458561800021
- [14] Y. Chai, K. Liu, C. Li, Z. Sun, L. Jin, and T. Shi, "A novel method based on long short term memory network and discrete-time zeroing neural algorithm for upper-limb continuous estimation using sEMG signals," *Biomedical Signal Processing and Control*, vol. 67, 2021, doi: 10.1016/j.bspc.2021.102416.
- [15] S. Stapornchaisit, Y. Kim, A. Takagi, N. Yoshimura, and Y. Koike, "Finger Angle Estimation From Array EMG System Using Linear Regression Model With Independent Component Analysis," *Frontiers in Neurorobotics*, vol. 13, 2019, doi: 10.3389/fnbot.2019.00075.
- [16] C. Chen, Y. Yu, X. Sheng, and X. Zhu, "Non-Invasive Analysis of Motor Unit Activation During Simultaneous and Continuous Wrist Movements," *IEEE Journal of Biomedical and Health Informatics*, vol. 26, no. 5, pp. 2106-2115, 2022, doi: 10.1109/jbhi.2021.3135575.
- [17] J. G. Ngeo, T. Tamei, and T. Shibata, "Continuous and simultaneous estimation of finger kinematics using inputs from an EMG-to-muscle activation model," *Journal of Neuroengineering and Rehabilitation*, vol. 11, Aug 2014, Art no. 122, doi: 10.1186/1743-0003-11-122.
- [18] M. Beretta-Piccoli, G. Boccia, T. Ponti, R. Clijsen, M. Barbero, and C. Cescon, "Relationship between Isometric Muscle Force and Fractal Dimension of Surface Electromyogram," *Biomed Research International*, vol. 2018, 2018, Art no. 5373846, doi: 10.1155/2018/5373846.
- [19] J. L. Dideriksen, D. Farina, and R. M. Enoka, "Influence of fatigue on the simulated relation between the amplitude of the surface electromyogram and muscle force," *Philosophical Transactions of the Royal Society a-Mathematical Physical and Engineering Sciences*, vol. 368, no. 1920, pp. 2765-2781, Jun 2010, doi: 10.1098/rsta.2010.0094.
- [20] J. J. Woods and B. Biglandritchie, "LINEAR AND NON-LINEAR SURFACE EMG FORCE RELATIONSHIPS IN HUMAN MUSCLES AN ANATOMICAL FUNCTIONAL ARGUMENT FOR THE EXISTENCE OF BOTH," *American Journal of Physical Medicine & Rehabilitation*, vol. 62, no. 6, pp. 287-299, 1983. [Online]. Available: <Go to ISI>://WOS:A1983RV10000002.

- [21] T. J. Roberts and A. M. Gabaldón, "Interpreting muscle function from EMG:: lessons learned from direct measurements of muscle force," *Integrative and Comparative Biology*, vol. 48, no. 2, pp. 312-320, Aug 2008, doi: 10.1093/icb/icn056.
- [22] P. Zhou and W. Z. Rymer, "Factors governing the form of the relation between muscle force and the EMG: A simulation study," *Journal of Neurophysiology*, vol. 92, no. 5, pp. 2878-2886, Nov 2004, doi: 10.1152/jn.00367.2004.
- [23] T. Sadamoto, F. Bondepetersen, and Y. Suzuki, "SKELETAL-MUSCLE TENSION, FLOW, PRESSURE, AND EMG DURING SUSTAINED ISOMETRIC CONTRACTIONS IN HUMANS," European Journal of Applied Physiology and Occupational Physiology, vol. 51, no. 3, pp. 395-408, 1983, doi: 10.1007/bf00429076.
- [24] R. Merletti and G. L. Cerone, "Tutorial. Surface EMG detection, conditioning and pre-processing: Best practices," *Journal of Electromyography and Kinesiology*, vol. 54, Oct 2020, Art no. 102440, doi: 10.1016/j.jelekin.2020.102440.
- [25] C. J. De Luca, L. D. Gilmore, M. Kuznetsov, and S. H. Roy, "Filtering the surface EMG signal: Movement artifact and baseline noise contamination," *Journal of Biomechanics*, vol. 43, no. 8, pp. 1573-1579, May 2010, doi: 10.1016/j.jbiomech.2010.01.027.
- [26] J. Piskorowski, "Time-efficient removal of power-line noise from EMG signals using IIR notch filters with non-zero initial conditions," *Biocybernetics and Biomedical Engineering*, vol. 33, no. 3, pp. 171-178, 2013, doi: 10.1016/j.bbe.2013.07.006.
- [27] R. N. Khushaba and K. Nazarpour, "Decoding HD-EMG Signals for Myoelectric Control-How Small Can the Analysis Window Size be?," *Ieee Robotics and Automation Letters*, vol. 6, no. 4, pp. 8569-8574, Oct 2021, doi: 10.1109/lra.2021.3111850.
- [28] A. Phinyomark, P. Phukpattaranont, and C. Limsakul, "Feature reduction and selection for EMG signal classification," *Expert Systems with Applications*, vol. 39, no. 8, pp. 7420-7431, Jun 2012, doi: 10.1016/j.eswa.2012.01.102.
- [29] M. Zardoshti-Kermani, B. C. Wheeler, K. Badie, and R. M. Hashemi, "EMG feature evaluation for movement control of upper extremity prostheses," *IEEE Trans. Rehabil. Eng. (USA)*, vol. 3, no. 4, pp. 324-333, Dec. 1995, doi: 10.1109/86.481972.
- [30] G. Liu and J. Wang, "EEGG: An Analytic Brain-Computer Interface Algorithm," *Ieee Transactions on Neural Systems and Rehabilitation Engineering*, vol. 30, pp. 643-655, 2022, doi: 10.1109/tnsre.2022.3149654.
- [31] G. Liu, "It may be time to perfect the neuron of artificial neural network," *IEEE TechRxiv*, 2023, https://doi.org/10.36227/techrxiv.12477266.
- [32] C. Luo, J. Wang, and Q. Miao, "Transient Current Ratio Dendrite Net for High-Resistance Connection Diagnosis in BLDCM," *IEEE Trans. Power Electron*.

- (*USA*), vol. 39, no. 4, pp. 4746-4757, 2024 2024, doi: 10.1109/tpel.2024.3356069.
- [33] G. Liu and J. Wang, "Dendrite Net: A White-Box Module for Classification, Regression, and System Identification," *IEEE Transactions on Cybernetics*, vol. 52, no. 12, pp. 13774-13787, 2022, doi: 10.1109/tcyb.2021.3124328.
- [34] G. Liu and J. Wang, "A relation spectrum inheriting Taylor series: muscle synergy and coupling for hand," *Frontiers of Information Technology & Electronic Engineering*, vol. 23, no. 1, pp. 145-157, Jan 2022, doi: 10.1631/fitee.2000578.
- [35] D. Yarotsky, "Error bounds for approximations with deep ReLU networks," *Neural Networks*, vol. 94, pp. 103-114, Oct 2017, doi: 10.1016/j.neunet.2017.07.002.
- [36] A. Pinkus, "Approximation theory of the MLP model in neural networks," *Acta Numer. (UK)*, vol. 8, pp. 143-195, 1999 1999, doi: 10.1017/s0962492900002919.
- [37] G. Liu, Y. J. Pang, S. Yin, X. K. Niu, J. Wang, and H. Wan, "Dendrite Net with Acceleration Module for Faster Nonlinear Mapping and System Identification," *Mathematics*, vol. 10, no. 23, Dec 2022, Art no. 4477, doi: 10.3390/math10234477.

- [38] J. M. Hahne *et al.*, "Linear and Nonlinear Regression Techniques for Simultaneous and Proportional Myoelectric Control," *Ieee Transactions on Neural Systems and Rehabilitation Engineering*, vol. 22, no. 2, pp. 269-279, Mar 2014, doi: 10.1109/tnsre.2014.2305520.
- [39] N. Jiang, H. Rehbaum, I. Vujaklija, B. Graimann, and D. Farina, "Intuitive, Online, Simultaneous, and Proportional Myoelectric Control Over Two Degrees-of-Freedom in Upper Limb Amputees," *Ieee Transactions on Neural Systems and Rehabilitation Engineering*, vol. 22, no. 3, pp. 501-510, May 2014, doi: 10.1109/tnsre.2013.2278411.
- [40] C. E. Lang and M. H. Schieber, "Human finger independence: Limitations due to passive mechanical coupling versus active neuromuscular control," *Journal of Neurophysiology*, vol. 92, no. 5, pp. 2802-2810, Nov 2004, doi: 10.1152/jn.00480.2004.
- [41] C. Häger-Ross and M. H. Schieber, "Quantifying the independence of human finger movements:: Comparisons of digits, hands, and movement frequencies," *Journal of Neuroscience*, vol. 20, no. 22, pp. 8542-8550, Nov 2000, doi: 10.1523/jneurosci.20-22-08542.2000.